Since January 2020 Elsevier has created a COVID-19 resource centre with free information in English and Mandarin on the novel coronavirus COVID-19. The COVID-19 resource centre is hosted on Elsevier Connect, the company's public news and information website.

Carbohydrate Polymers 264 (2021) 118011

Contents lists available at ScienceDirect

Carbohydrate Polymers

journal homepage: www.elsevier.com/locate/carbpol

Sulfobutylether-beta-cyclodextrin-enabled antiviral remdesivir: Characterization of electrospun- and lyophilized formulations

Lajos Szente [a,*], István Puskás [a], Tamás Sohajda [a], Erzsébet Varga [a], Panna Vass [b], Zsombor Kristóf Nagy [b], Attila Farkas [b], Bianka Várnai [c], Szabolcs Béni [c], Eszter Hazai [d]

[a] CycloLab Cyclodextrin R&D Laboratory Ltd., H-1097, Budapest, Illatos út 7., Hungary
[b] Budapest University of Technology and Economics, H-1111, Budapest, Műegyetem rkp. 3, Hungary
[c] Semmelweis University, Department of Pharmacognosy, Budapest, Üllői út 26, Hungary
[d] Virtua Drug, Ltd., H-1015, Budapest, Csalogány utca 4C, Hungary

ARTICLE INFO

Keywords:
Remdesivir
Solubilization
Sulfobutylether-beta-cyclodextrin
Inclusion
Electrostatic interaction
X-ray diffraction
Differential scanning calorimetry
RAMAN-mapping
2D ROESY NMR

ABSTRACT

Veklury™ by Gilead Sciences, Inc., containing antiviral drug, remdesivir (REM) has received emergency authorization in the USA and in Europe for COVID-19 therapy. Here, for the first time, we describe details of the non-covalent, host-guest type interaction between REM and the solubilizing excipient, sulfobutylether-beta-cyclodextrin (SBECD) that results in significant solubility enhancement. Complete amorphousness of the cyclodextrin-enabled REM formulation was demonstrated by X-ray diffraction, thermal analysis, Raman chemical mapping and electron microscopy/energy dispersive spectroscopy. The use of solubilizing carbohydrate resulted in a 300-fold improvement of the aqueous solubility of REM, and enhanced dissolution rate of the drug enabling the preparation of stable infusion solutions for therapy. 2D ROESY NMR spectroscopy provided information on the nature of REM–excipient interaction and indicated the presence of inclusion phenomenon and the electrostatic attraction between anionic SBECD and nitrogen-containing REM in aqueous solution.

1. Introduction

Remdesivir (GS-5734), was discovered and developed by Gilead Sciences, Inc. It has recently been introduced as a promising new antiviral agent for the therapy against SARS-CoV-2 in the form of a marketed product, named Veklury™.

Initially, this compound was designed and developed to fight hepatitis C and Ebola virus disease. Since January 2020, REM has been administered to dozens of early- and late-phase clinical trials worldwide. Published clinical reports of these trials have shown promising, but sometimes turbulent efficacy patterns (Grein, Ohmagari, & Shin, 2020; Siegel, Hui, & Doerffler, 2017). Chemically, REM is a monophosphoramidate prodrug. (Fig. 1).

REM has broad antiviral activity against RNA viruses, including filoviruses (Ebola and Marburg) and coronaviruses, such as severe acute respiratory syndrome coronavirus (SARS-CoV), Middle East respiratory syndrome coronavirus (MERS-CoV), and SARS-CoV-2. This prodrug is metabolically transformed by intracellular esterases and kinases to the pharmacologically active nucleoside, a triphosphate analogue (GS-443902). The active metabolite competes with adenosine phosphate and acts as an RNA-dependent RNA polymerase inhibitor (Agostini et al., 2018).

REM exhibits potent *in vitro* activity against SARS-CoV-2 with an half-maximal effective concentration of 0.77 μM (Gordon, Tchesnokov, Feng, Porter, & Gotte, 2020; Wang et al., 2020).

Due to the high first pass liver metabolism of phosphoramidates and low oral bioavailability, REM cannot be administered orally (Cao, Deng, & Dai, 2020). Therefore an intravenous infusion in the form of a parenteral solution remained the only administration route of REM. Infusion drug formulations are ideally clear, stable aqueous solutions of the active ingredient. However, REM is poorly soluble in water. Due to its limited aqueous solubility (0.028 mg/mL at room temperature), a need arose for solubility enhancement. This was attempted by employing different solubilizer excipients, such as surfactants, polymers, co-solvents and sulfobutylether-beta-cyclodextrin (SBECD). The 20 % (w/w) aqueous solutions of Tween-80 provided 3.9 mg/mL dissolved REM, the PEG-400, dissolved 3.3 mg/mL, while the SBECD at this concentration resulted in 8.5 mg/mL dissolved REM (Larson, 2019).

* Corresponding author.
E-mail address: szente@cyclolab.hu (L. Szente).

https://doi.org/10.1016/j.carbpol.2021.118011
Received 28 January 2021; Received in revised form 22 March 2021; Accepted 28 March 2021
Available online 7 April 2021

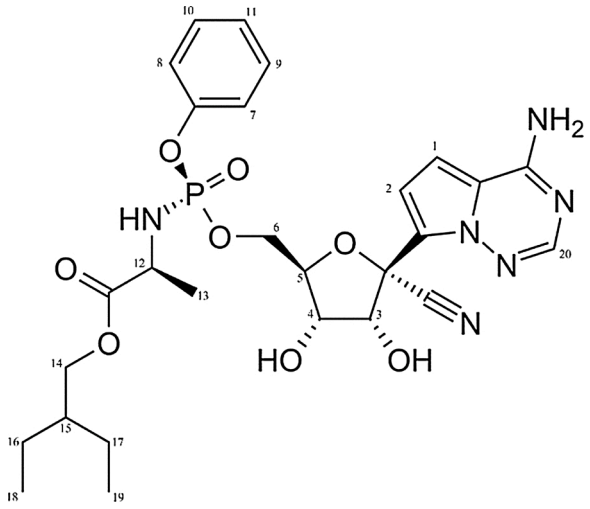

Fig. 1. Structure and numbering of REM.

The application of surfactants and polymers - despite their solubility enhancing effect - was found inadequate for enough active ingredient for a preferred formulation.

The only satisfactory solubility enhancement was achieved by using sulfobutylether-beta-cyclodextrin (SBECD). Currently, 13 FDA-approved injectable products are on the market that contain SBECD solubilizing excipient and numerous clinical candidates are under development (Stella & Rajewski, 2020).

SBECD is a highly water-soluble amorphous solid. It is a multicomponent blend composite, an isomeric mixture of negatively charged cyclodextrin derivatives in the form of sodium salts. The average degree of substitution is 6.5 sulfobutyl-groups per beta-cyclodextrin ring. The distribution of the sulfobutyl groups on the primary and secondary side of the cyclodextrin torus is statistically random (Loftsson & Brewster, 2010; Szente & Szejtli, 1999). The present paper aims at the detailed physico-chemical characterization of cyclodextrin-enabled REM formulations in the solid state and in aqueous solution, using diverse analytical and spectroscopic methods. The characteristics of electrospun nanofiber and freeze-dried forms of the SBECD-enabled REM are compared.

2. Experimental

2.1. Materials

Remdesivir (REM) with a chemical purity of 99.2 % was purchased from Echemi Pharma, Qingdao, China.

Sulfobutylether-beta-cyclodextrin (SBECD) Dexolve™ (USP Betadex Sulfobutyl Ether Sodium) was a product of CycloLab, Budapest, Hungary. Five commercially available SBECD samples from different sources were involved in the comparative solubility enhancement studies and used as received. All these samples met the quality requirements set for pharmaceutical grade USP Betadex Sulfobutyl Ether Sodium – SBECD. The samples will be marked as source No. 1.-2.-3.-4.-5.

2.2. SBECD-assisted solubilization of REM

The SBECD samples of different origin were dissolved in purified water (taking their corresponding water content into consideration) and their pH was set to the value of 1.9 with hydrochloric acid. The same amount of REM was added to each of these solutions in excess and stirred for 24 h at room temperature to attain equilibrium. The resulting suspensions were filtered through 0.45 μm pore size membrane syringe filters and the isolated solution phase was assayed for dissolved REM concentration by HPLC.

2.3. Preparation of Dexolve-enabled REM binary formulations

Two types of formulations with identical composition were prepared and investigated. Common aqueous solutions of REM and SBECD were made at room temperature. The solutions were filtered across a 0.22 μm membrane. The resulting clear filtrates were processed by lyophilization and electrospinning into solid binary formulations. Previous observations indicated that reconstitution properties of SBECD-voriconazole electrospun nanofibre solid formulation surpassed those of the corresponding lyophilizate (Vass et al., 2019). This study aimed at the comparison of wettability and dissolution properties of freeze-dried and electrospun nanofiber formulations of SBECD-enabled REM.

2.3.1. Preparation of the freeze-dried formulation

An aqueous solution was prepared by dissolving 9.56 g SBECD (equivalent to 9.00 g dry SBECD) in 17.4 mL deionized water at room temperature. The pH of the solution was set to 1.9 by adding 50 μL of 1.0 M hydrochloric acid. Then 300 mg REM was added to the acidified SBECD solution upon continuous agitation for 2 h at room temperature. The REM showed poor wetting in the SBECD solution, intense agitation was necessary to get it homogenized. The final pH of the resulting solution was adjusted to 3.5 by adding 100 μL of 1.0 M NaOH solution. The solution was cooled down on dry ice/ethanol mixture to -55 °C and lyophilized. The process yielded 9.6 g of white, fluffy amorphous solid.

2.3.2. Preparation of electrospun nanofiber formulation

Electrospinning was carried out using a high-speed electrospinning setup consisting of a stainless-steel spinneret (d =34 mm) connected to a high-speed motor. The spinneret was equipped with orifices (d =330 μm). The REM-SBECD complex solution was fed with a SEP-10 S Plus syringe pump with a flow rate of 100 mL/h. The rotation rate of the spinneret and the applied voltage were 40,000 rpm and 40 kV, respectively. Electrospinning was performed at ambient temperature (25 °C). The produced fibers were collected by a cyclone. For electrospinning, 28.834 g of SBECD (corrected with its 6.5 % residual water content, it is equivalent to 26.997 g) was dissolved in 10.9 mL of deionized water at room temperature. The resulting solution was acidified with 1.37 mL 2.0 M hydrochloric acid, to attain pH 1.8 for the solution. To this acidic SBECD solution, 0.900 g REM was added under continuous stirring. The pH of the resulting REM-SBECD solution was adjusted to pH 3.2 with 0.53 mL 2.0 M NaOH. This solution was then processed with high-speed electrospinning to get the electrospun nanofibers. This yielded 20 g REM-SBECD nanofiber.

2.4. Characterization of REM-SBECD formulations

2.4.1. HPLC method

An Agilent 1260 HPLC system equipped with diode-array detector (DAD) was used to identify and quantitate REM. Reversed-phase separation was achieved on a Kinetex C18 analytical column (Phenomenex Inc., Torrance, CA, USA) with 100 mm length, 4.6 mm internal diameter and 2.6 μm particle size. using a solvent gradient of water with 0.05 % formic acid with acetonitrile with 0.05 % (0 min 0 %, 10 min 100 %) at a flow rate of 0.8 mL/min and UV-diode array (DAD) detection at 240 nm wavelength.

2.4.2. X-ray powder diffraction

Powder X-ray diffraction patterns were recorded with a X'pert Pro MDP (PANalytical B.v., The Netherlands) X-ray diffractometer using CuK_{α} radiation and Ni filter.

2.4.3. Differential scanning calorimetry

The measurements were performed using a Modulated DSC 2920 device (TA Instruments, DE, USA) under inert gas atmosphere. The samples (1−5 mg) were weighed in sealed Al-pans at a heating rate of 10 K/min. For temperature and enthalpy calibration of the DSC instrument,

a pure indium metal standard was applied.

2.4.4. Scanning electron microscopy (SEM) and energy dispersive spectroscopy (EDS)

Morphology of the samples was investigated by a JEOL 6380LVa (JEOL, Tokyo, Japan) type scanning electron microscope. Each specimen was fixed with conductive double-sided carbon adhesive tape and sputter-coated with gold prior to the examination to avoid electrostatic charging. The applied accelerating voltage and working distance were 15 kV and 10 mm, respectively. Energy dispersive spectrometry (EDS) was used in conjunction with SEM for the mapping of sodium, sulfur, and phosphorus in the samples. The detected X-ray radiation was between 4000 and 5000 counts/s.

2.4.5. Raman chemical mapping

For Raman chemical mapping Horiba Jobin Yvon, Labram type Raman micro-spectrometer instrument was used. Samples were investigated by Olympus BX-40 optical microscope coupled with Nd-YAG solid state laser spectrometer. Registration of spectra were made using 50-fold magnification objective. Data collection and processing were done by a Labspec 5 computer software. Spectra of reference REM and SBECD samples were recorded by a point measurement. The investigation of solid binary formulations was done by scanning larger sample surfaces *via* a motorized stage.

2.5. NMR spectroscopic characterization of REM-SBECD in solution

Nuclear magnetic resonance (NMR) spectroscopy measurements were carried out on a 600 MHz Varian DDR NMR spectrometer (Agilent Technologies, Palo Alto, CA, USA), equipped with a 5 mm inverse-detection gradient probehead. Standard pulse sequences and processing routines available in VnmrJ 3.2C/Chempack 5.1 were used. The complete resonance assignments of REM and the partial assignment of SBECD were established from direct ^{1}H–^{13}C, long-range ^{1}H–^{13}C, and scalar spin-spin connectivities derived from 1D ^{1}H, 2D ^{1}H-^{1}H gCOSY, zTOCSY (mixing time of 150 ms), ROESY (mixing time of 300 ms) and ^{1}H–^{13}C gHSQCAD (J =140 Hz) experiments. The ^{1}H chemical shifts were referenced to the methyl singlet (δ =3.31 ppm) of internal CH_3OH, a reference substance without any possible interaction with the cyclodextrins.

2.5.1. ^{1}H NMR titration experiments

The stoichiometry of REM complexation with SBECD was investigated by Job's method of continuous variation (Job, 1928). Samples were prepared in acidic (D_2O, HCl; pD 2.0) solutions at 298 K. The total molar concentration of the host and guest components $c_{REM} + c_{SBECD}$ was kept constant at 1.0 mM, while the mole fraction of REM, $x_{REM} = c_{REM} / (c_{REM} + c_{SBECD})$ was varied gradually in 0.1 unit steps from 0 to 1. ^{1}H chemical shifts δ^{REM} were recorded at 600 MHz for several REM resonances and complexation-induced displacement values, $\Delta\delta^{REM} = |\delta^{REM} - \delta_{REM}|$ were calculated with respect to δ_{REM} measured in the absence of SBECD. To construct Job's plots, $\Delta\delta^{REM}$ values were multiplied by the mole fraction of REM and depicted as a function of x_{REM}.

To determine the complex stability constant a separate NMR titration was performed at pD 2.0. The titration with SBECD was constructed as follows: 500 µL of 1.0 mM REM solution was titrated with a 6.16 mM SBECD stock solution (up to 500 µL in various portions). Following equilibration, ^{1}H NMR spectra were recorded in each titration step at 298 K. Titration datasets were analyzed by the following method: the experimental titration curves for well-resolved resonances of REM were evaluated by the O scientific visualization software, by assuming the formation of 1:1 REM·SBECD complex (according to the Job's plot result). If complexation occurs with rapid kinetics on the NMR chemical shift timescale, the observed chemical shift $\delta^{obs}_{REM,\,i}$ of the ith carbon-bound proton in REM becomes a mole-fraction weighted average (Fielding, 2000) of the species-specific values in the uncomplexed REM ($\delta^{REM,\,i}$) and in the complex ($\delta^{REM\cdot CD,\,i}$),

$$\delta^{obs}_{REM,\,i} = \frac{\delta^{REM,\,i} \cdot c_{REM} + \delta^{REM\cdot SBECD,\,i} \cdot c_{REM\cdot SBECD}}{c^{REM}_{total}} \quad (1)$$

where $c_{REM\cdot SBECD}$ and c_{REM} denote equilibrium concentrations, while c^{REM}_{total} is the total concentration of the compounds in the solution.

Chemical shifts for all resonances (i) of REM were plotted as a function of V_{SBECD} (µL) to select the resonances with sufficient sensitivity ($\Delta\delta$) to enter the evaluation in order to determine the complex stability constant (log$K$) value.

2.5.2. NMR structural study of complex formation

To explore the spatial arrangement of the host-guest complexes and identify the interacting molecular sequences, nuclear Overhauser effect (NOE) type experiments were performed on a 1:1 molar ratio REM : SBECD sample under acidic conditions (pD 2.0), at 298 K. NOE is a manifestation of dipolar cross relaxation between two nonequivalent nuclear spins that are close enough (< 5 Å) in space (Neuhaus & Williamson, 2000). The NOE intensities are scaled with r^{-6}, where r represents the mean distance between the protons. 2D ROESY spectra were acquired collecting 16 scans on 1258 × 512 data points, applying a mixing time of 300 ms.

2.6. Reconstitution properties of freeze dried and electrospun nanofiber formulations

For comparison of wettability and redissolution of SBECD-REM formulations, identical composition of physical mixture and the two investigational formulations of REM and SBECD were studied. The physical mixture was prepared by weighing and homogenizing 100 mg REM and 3000 mg Dexolve SBECD dry powders. The lyophilizate and the electrospun sample contained the constituents in the same weight ratio. 980 mg of each the physical mixture, the lyophilizate and finely ground electrospun sample were weighed in three separate beakers and 6.0 mL of **w**ater **f**or **i**njections (WFI) was added to these powders. The spontaneous dissolution was followed by visual inspection and photographed as a function of at room temperature without agitation.

2.7. Molecular docking calculations

Initial coordinates of BCD were extracted from a published X-ray structure of a CD–protein complex (Kondo, Ohtaki, Tonozuka, Sakano, & Kamitori, 2001). Initial 3D coordinates of SBECD were built using Chemaxon tools based on BCD crystal structure. In the course of molecular docking calculations, the number of random substitutions on beta-cyclodextrin was kept at 6 as the average substitution degree of SBECD is 6.5 sulfobutyl-groups per beta-cyclodextrin ring. Initial coordinates of REM were built and optimized using Marvin software (Chemaxon Inc, Budapest, Hungary). Semiempirical energy minimization and calculation of partial charges were performed for further minimization purposes using the PM6 method by MOPAC2009 package. Molecular docking calculations were carried out using the Autodock Vina software integrated in the Molecular Docking Server (http://www.dockingserver.com) (Bikadi & Hazai, 2009; Trott & Olson, 2010). Water molecules and heteroatoms were removed from the structures, since water is implicitly included in Autodock. Simulation boxes were centered on cyclodextrin. A simulation box of 22 × 22 × 22 Å was used in each docking calculation with an exhaustiveness option of 8 (average accuracy).

Table 1
Equilibrium solubility of REM in 20 % (w/w) of aqueous solution of pH 1.9 of SBECD from different manufacturers at 25 °C.

Source of SBECD	REM in solution (mg/mL)
source No. 1	8.34
source No. 2	7.91
source No. 3	8.55
source No 4.	7.62
source No 5.	8.23
Dexolve™ SBECD	9.73

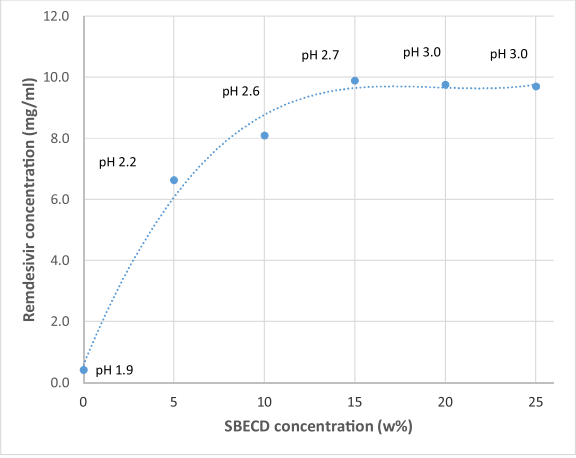

Fig. 2. Solubility isotherm of REM in acidic Dexolve™ SBECD solutions at 25 °C.

3. Results and discussions

3.1. SBECD-assisted solubilization of REM

Maximum attainable solubility of REM in 20 % (w/w) aqueous solutions of commercially available SBECD from different manufacturers was found to be in the range of 7.6–9.7 mg/mL as determined by HPLC (Table 1). The pH of the equilibrium solutions after membrane filtration fell between values 3.0 and 3.1.

The 20 % aqueous solutions of SBECD from different sources provided a significant solubility enhancement of REM (average 8.4 mg/mL) in acidic conditions at room temperature. All SBECDs used in this experiment, greatly surpassed the solubilization power of both 20 % Tween 80 (3.9 mg/mL REM) and 20 % PEG-400 (3.3 mg/mL REM) under identical coditions. The solubility of REM in acidic aqueous solutions of various concentrations of Dexolve™ SBECD was also studied. The obtained phase solubility curve is shown in Fig. 2.

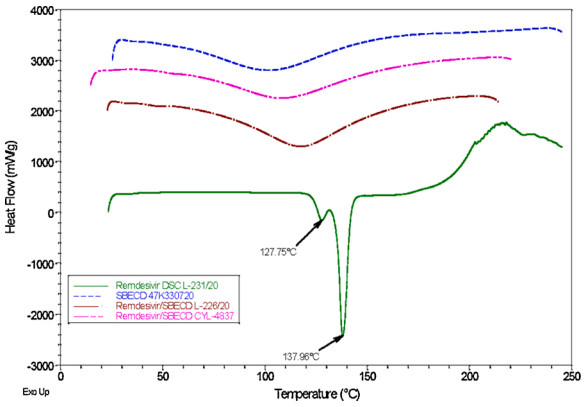

Fig. 4. Overlaid DSC thermograms of REM (green), Dexolve SBECD (blue), REM/SBECD freeze-dried form (purple) and REM/SBECD electrospun nanofiber (brown).

A peculiar type of solubility isotherm was obtained for solutions of multivariate pH values. It has to be noted herein that SBECD itself has no buffering capacity. Throughout the solubilization test our team has refrained from using any added buffering agent since for the purpose of pH setting in the marketed finished dosage form exclusively HCl and NaOH are used. The initial pH values of the used SBECD solutions were – however – identically set to pH 1.9 with HCl. Along with the increasing dissolved REM concentrations, the pH of the solutions also reached higher values up to pH 3.0. At this pH, further increase of the SBECD concentration did not result in additional solubilizing potential of the dissolution medium. Reconstituted Veklury™ lyophilized powder for concentrate contains REM in 5 mg/mL concentration, the solubility isotherm well illustrates that nearly 100 % cyclodextrin excess (related to the saturated solution) may adequately ensure the physical stability of the reconstituted solution in the marketed product.

3.2. Appearance and composition of solid REM-SBECD formulations

Both the lyophilized and electrospun nanofibre formulation of SBECD-REM appear white fluffy amorphous, glassy solids. The REM contents of the SBECD-enabled REM formulations were determined by HPLC. The HPLC method developed was found suitable for the identification and quantitation of REM and detection of its degradation products. The REM load of the lyophilisate was fond 3.23 % by weight. The electrospun SBECD-REM formulation had 3.22 % REM content by weight. The composition of both formulations was identical with that of the marketed Veklury™ product developed by Gilead Sciences.

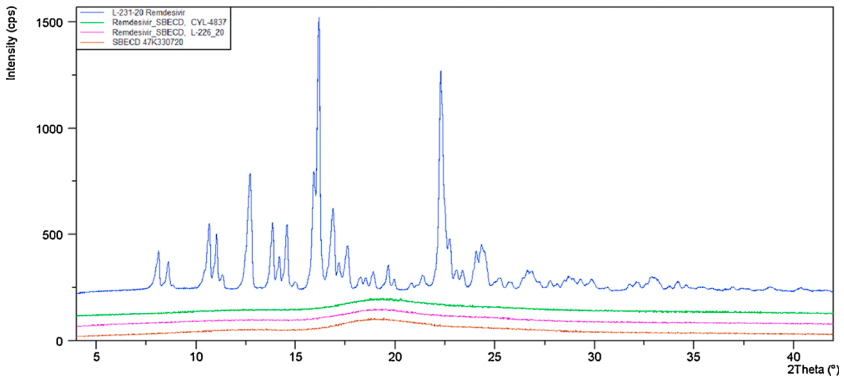

Fig. 3. Overlaid X-ray powder diagrams of REM (blue), Dexolve SBECD (brown), REM/SBECD freeze-dried form (purple) and REM/SBECD electrospun nanofiber (green).

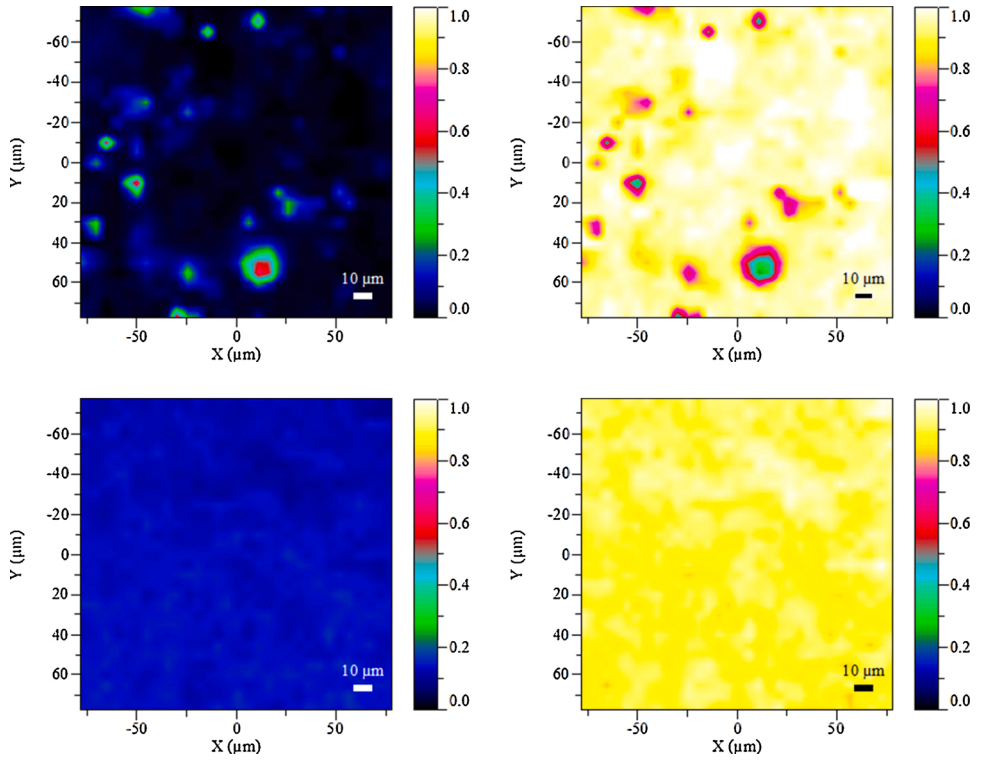

Fig. 5. Raman mapping patterns of physical mixture of REM + SBECD (upper pictures) and of REM/SBECD freeze-dried formulation (bottom pictures). Legend: Blue patterns on the left refer to REM distribution, yellow patterns ont he right refer to SBECD distribution.

3.3. Solid phase properties of REM and its SBECD-enabled formulations

3.3.1. X-ray powder diffraction pattern

Freeze-drying and electrospinning of the aqueous solutions of binary REM-SBECD composition have resulted in solid formulations that appear entirely amorphous, with no signs of any crystallinity of REM (see Fig. 3).

3.3.2. Thermoanalytical characterization of REM and SBECD-enabled formulations

The results of X-ray diffraction patterns indicated complete amorphousness of the cyclodextrin-enabled REM formulations due to the molecular entrapment of REM. These crystallographic observations were supported by thermoanalytical investigations. (Fig. 4)

The crystalline nature of the REM is clearly shown by the melting enthalpy heat-flow curves at 127 and 137 °C, respectively. It is noteworthy that two distinct melting points were detected by DSC, probably due to the coexistence of different REM polymorphs. Similarly to the X-ray diffraction pattern of SBECD, and the SBECD-enabled solid REM formulations, no well-defined melting point was detected demonstrating the amorphous nature of the excipient and the two REM binary formulations.

3.3.3. Raman chemical mapping

Raman microscopy-based chemical mapping of the physical mixture containing 3.2 % REM and 96.8 % SBECD provided distribution patterns for REM in a bulk carbohydrate matrix. This technique clearly demonstrated heterogeneity when the crystalline REM was distributed as a physical mixture. However, the solid forms of the inclusion complex with the same average composition were found to have the drug evenly distributed in the SBECD excipient. Not even micro-heterogeneity was detected for REM cyclodextrin formulations. (Fig. 5)

3.3.4. SEM-EDS micrographs

SEM- and EDS investigations were conducted to assess the distribution homogeneity of REM in the cyclodextrin matrix. The working principle of this EM-technique is that the element phosphorus in the REM molecule can be used to differentiate the active ingredient from SBECD that does not contain phosphorus. However, the element sulfur is a constituent of SBECD, whereas the REM molecule does not contain sulfur. The false colors selected for the EDS maps were red representing phosphorus- and blue indicating sulfur-containing species.

Fig. 6 shows elemental maps of the physical mixture, the lyophilized- and electrospun nanofiber forms the REM-SBECD binary systems, respectively. The images reveal that the physical mixture contains separate SBECD and REM particles, the active ingredient is distributed

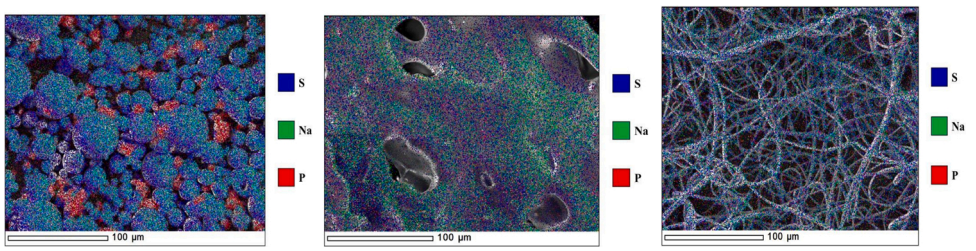

Fig. 6. SEM-EDS micrographs of physical mixture (left) the lyophilized (middle) and electrospun nanofiber form (right) of REM-SBECD formulations.

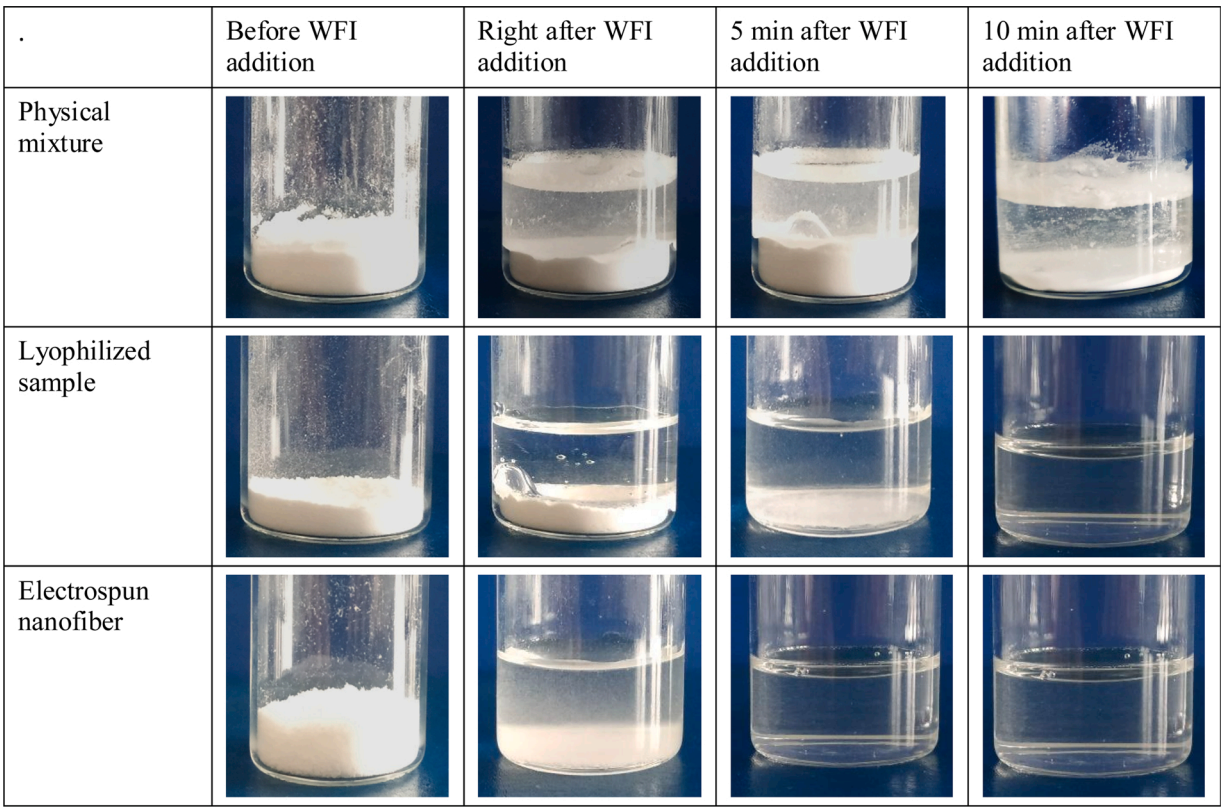

Fig. 7. Reconstitution properties of 980 mg REM-SBECD binary systems: physical mixtures freeze-dried and electrospun nanofiber complexes in 6 mL of deionized water.

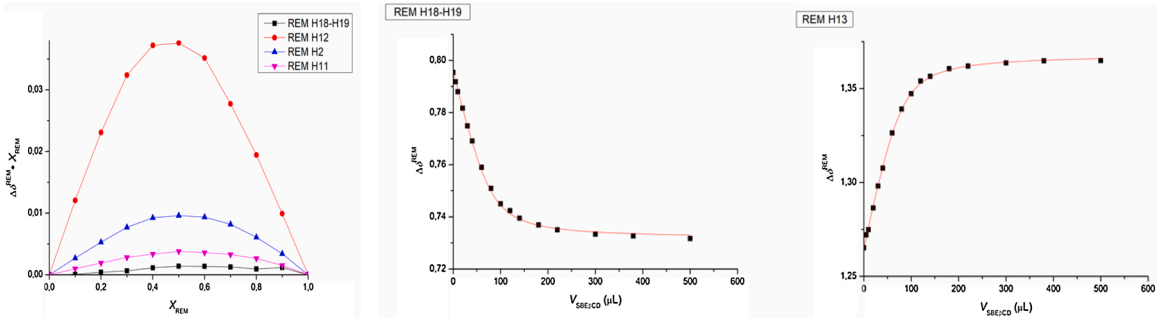

Fig. 8. Job's plot of the observed ^{1}H resonances of REM throughout complexation with SBECD (left graph) and selected titration profiles of observed REM protons (H18-H19 and H13), simultaneously fitted by the 1:1 complexation model using the Origin program (middle and right graph.).

unevenly in the carbohydrate matrix, whereas the electrospun sample and the lyophilized REM-SBECD powder contain both the excipient and REM evenly distributed. No larger aggregates of REM in the freeze-dried complex or in electrospun nanofiber formulation are detected. These examinations suggest that the REM active drug is molecularly dispersed both in the electrospun fibers and the freeze-dried complex.

3.4. Reconstitution properties of SBECD-enabled REM in water

Fig. 7. demonstrates the differences of wettability, dissolution rate and water solubility of the physical mixture of REM and SBECD compared with those of the two complex formulations (lyophilized and electrospun samples). The physical mixture did not dissolve completely, the partial dissolution of the composite powder could be attributed to the hydrophilic SBECD matrix. After 10 min measured from the addition of water, the lyophilized sample spontaneously dissolved. Full dissolution of the electrospun nanofibers was observed notably faster. The dissolution was completed in 5 min after contact with the dissolution medium. As shown in Fig. 7, significant differences were found in wettability and dissolution rates of formulations with identical average composition indicating that solid-phase engineering and complexation with SBECD matter.

3.5. NMR spectroscopic characterization of REM-SBECD in solution

3.5.1. ^{1}H NMR titration experiments

In order to assess the complexation stoichiometry, Job's plots were constructed from well-separated ^{1}H NMR signals (H18-H19, H12, H2, and H11) of REM. The Job's plot curve (left hand side graph of Fig. 8) shows a maximum at x_{REM}= 0.5, suggesting the formation of a single REM:SBECD complex with 1:1 stoichiometry.

To explore the binding affinity of REM to SBECD, a single-tube ^{1}H NMR titration of REM with SBECD was carried out. Chemical shift variation of the following REM resonances were monitored: H18-H19,

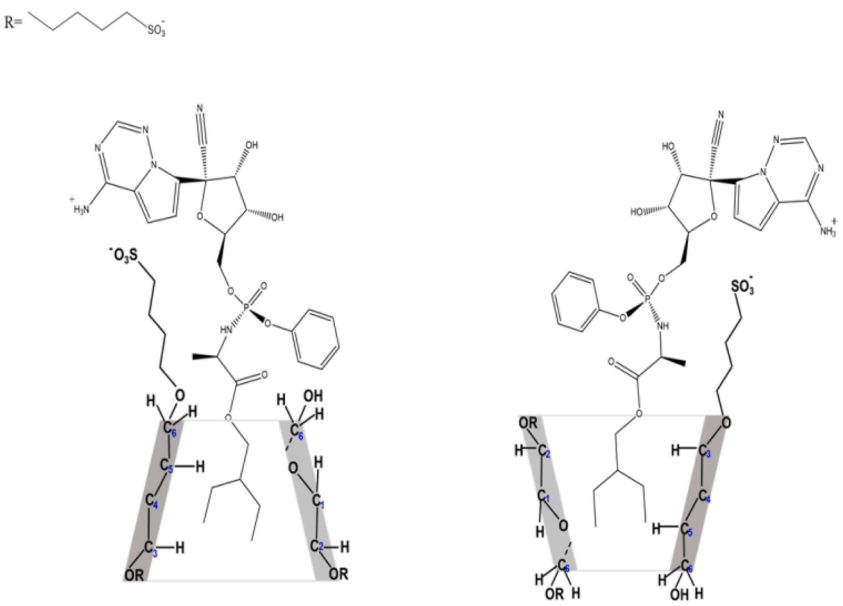

Fig. 9. Suggested structures of inclusion complexes for REM and SBECD in aqueous solution based on 2D NMR ROESY data at pD = 2.0.

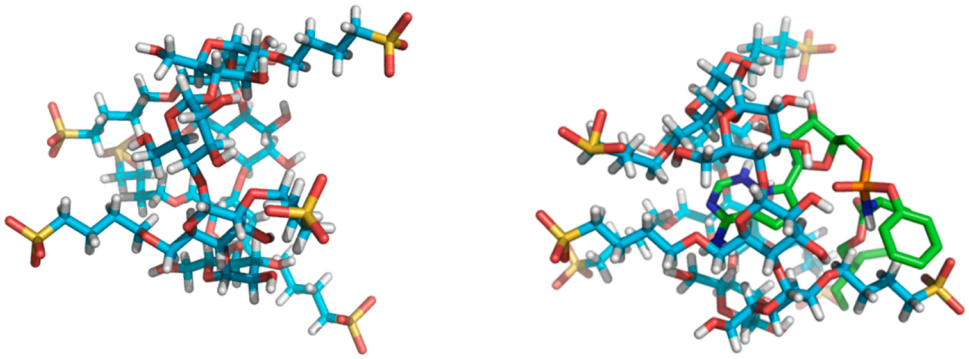

Fig. 10. Computer docking images of host guest interaction between SBECD and REM at neutral pH conditions:" empty" SBECD shown on the left molecular model while REM entrapped in SBECD is shown on the right hand side.

H13, H9-H10, and H1. Titration datasets were fitted by the 1:1 stoichiometry model for the REM·SBECD complex, as previously suggested by the Job's plots. In order, to extract a robust and reliable stability constant (Al-Soufi, Cabrer, Jover, Budal, & Tato, 2003), these four datasets were subjected to simultaneous nonlinear regression using the Origin software package (see right graph of Fig. 8). This global evaluation yielded log$K$ = 3.99 with an estimated standard deviation of 0.02, indicating a strong binding affinity for SBECD.

3.5.2. NMR structural study of REM-SBECD interaction

To obtain atomic-level information about the 3D structure of the complex, NOE experiments were carried out. A solution of REM : SBECD with 1:1 M ratio was tested. Spatial proximities between the ethyl-butyl sidechain of REM and SBECD could be deduced. ROESY cross-peaks could be detected between the diastereotopic methyl- (H18-H19) the methylene (H16-H17) resonances as well as the methine CH signals (H15) and the H3 resonance of the SBECD. This suggested that the aliphatic moiety was immersed into the cavity of the cyclodextrin. Much weaker interaction could be observed between the phenoxy-group resonances and the SBECD, however spatial proximity could not be assigned to any particular SBECD resonance. The host-guest type interaction was also confirmed by a further ROESY cross-peak between the methyl resonance of the alanyl residue (H13) and the methylenes of the CD's sulfobutyl sidechain. The inclusion geometry can therefore be further supported by an ionic interaction between the anionic host and the cationic guest (see Fig. 9). Finally, no intermolecular interaction could be observed between the heterocyclic moiety and the cyclodextrin in acidic solution. Unfortunately, the limited solubility of the non-ionized REM at pD 7.0 hindered the acquisition of 2D ROESY experiments.

3.6. Computer docking experiments

Docking calculations are carried out with implicit water model at pH 7.0. The lowest docking energy was calculated to be - 6.7 kcal/mol, which indicated the existence of a relatively stable inclusion complex. REM in its non-ionized form, was found to optimally fill the elongated nanocavity of SBECD, establishing a non-covalent host-guest type inclusion complex. As can be seen in the Fig. 10, at neutral pH the non-ionized form of REM penetrates into the cyclodextrin with its pyrrolo-triazine-amine ring filling the central cavity of SBECD (the lowest energy conformations show similar geometries, the only difference between these calculated geometries can be observed in the conformation of the flexible REM side chains). The polar side chains of SBECD form hydrogen bonds with the hydroxyl group of tetrahydrofuranyl and with the amino group of REM.

The above docking calculations were carried out with implicit water model at pH 7.0, however, the Veklury™ formulation contains REM and

SBECD in acidic pH solution. Therefore, the complex structure at such a low pH can be drastically different as compared to the structure of the host-guest complex at neutral pH, due to the ionisation of REM and the change in water structure. At acidic pH, the aliphatic chain was found to penetrate into the cyclodextrin cavity rather than the ionized *N*-heterocycle of REM, consistent with the above NMR experiments.

4. Conclusion

In the present study we aimed at the characterization of the non-covalent molecular interaction between the antiviral agent REM and a solubilizer excipient SBECD in the solid phase and in aqueous solution. Using X-ray diffraction and DSC thermal analysis, we demonstrated that the molecular entrapment of REM resulted in the complete amorphization of its crystalline structure both in the lyophilized and electrospun form. Raman chemical mapping and SEM-EDS provided independent evidence for the molecular dispersion and homogeneous distribution of REM in the carbohydrate excipient matrix.

The solubility study showed that REM can be solubilized in SBECD aqueous solutions reaching 7.6–9.7 mg/mL dissolved REM concentration, depending on the source of commercial SBECDs. The SBECD-enabled REM formulations are readily dissolved within a few minutes. Reconstitution and dissolution properties of electrospun nanofibre form of REM was found to outdo those of the lyophilized formulation having identical composition. These superior weeting and dissolution properties of electrospun nanofiber offer the possibility to develop non-invasive, quickly absorbable dosage forms of REM. Further studies are in progress to prove the feasibility of electrospun nanofiber made from SBECD-enabled REM as a non-invasive therapeutic option.

Detailed structural information was gained from the 2D ROESY NMR spectroscopy performed on the acidic aqueous solution of REM/SBECD formulation. We have shown that in an acidic solution REM resides inside the cavity of SBECD with its ethyl-butyl sidechain, while no inclusion phenomenon occurs between the positively charged heterocyclic moiety and SBECD. Besides the inclusion phenomenon, hydrogen bond-related and electrostatic interactions also play a role in the formation of the stable supramolecular complex. Computer docking experiments provided theoretical support of the molar stoichiometry of the host-guest type inclusion complex and mode of insertion of REM into the SBECD cavity under simulated neutral pH conditions in water. Our current observations are in an agreement with previously published data by Stella and coworkers (Okimoto, Rajewski, Uekama, Jona, & Stella, 1996) on the types of molecular interactions between neutral and charged drugs and SBECD polyanionic cyclodextrin derivative.

Authors contribution

L. S. conceptualized the study, compiled and edited manuscript, I. P. and T. S. work in formulation, interaction and solubility studies, E. V. the HPLC analyses, P. V. electrospinning, Zs. N and A. F. X-ray, DSC, Raman mapping, SEM-EDS, B.V and S.B. NMR experiments, E. H. molecular modeling, docking.

Declaration of Competing Interest

Authors declare no conflict of interest.

Acknowledgements

S. Beni is grateful for the financial support from the János Bolyai Research Scholarship of the Hungarian Academy of Sciences and from the Bolyai+New National Excellence Program (grant number: ÚNKP-20-5-SE-31) of the Ministry of Human Capacities. This work was supported by OTKA grant FK-132133 and by the ÚNKP-20-4New National Excellence Program of the Ministry for Innovation and Technology from the source of the National Research, Development and Innovation Fund.

References

Agostini, M. L., Andres, E. L., Sims, A. C., Graham, R. L., Sheahan, T. P., & Lu, X. (2018). Coronavirus susceptibility to the antiviral remdesivir (GS-5734) is mediated by the viral polymerase and the proofreading exoribonuclease. *mBio, 9*(2). https://doi.org/10.1128/mBio.00221-18

Al-Soufi, W., Cabrer, P. R., Jover, A., Budal, R. M., & Tato, J. V. (2003). Determination of second-order association constants by global analysis of 1H and 13C NMR chemical shifts. *Steroids, 68*, 43–53. https://doi.org/10.1016/s0039-128x(02) 00114-00119

Bikadi, Z., & Hazai, E. (2009). Application of the PM6 semi-empirical method of modeling proteins enhances docking accuracy of AutoDock. *Journal of Cheminformatics, 1*, 15. https://doi.org/10.1186/1758-2946-1-15

Cao, Y., Deng, X., & Dai, S. (2020). Remdesivir for severe acute respiratory syndrome coronavirus 2 causing COVID-19: An evaluation of the evidence. *Travel Medicine and Infectious Disease, 35*, Article 101647. https://doi.org/10.1016/j.tmaid.2020.101647, 2020 May-June.

Fielding, L. (2000). Determination of association constants (K(a)) from solution NMR data. *Tetrahedron, 56*, 6151–6170. https://doi.org/10.1016/S0040-4020(00)00492-0

Gordon, C. J., Tchesnokov, E. P., Feng, J. Y., Porter, D. P., & Gotte, M. (2020). The antiviral compound remdesivir potently inhibits RNA-dependent RNA polymerase from Middle East respiratory syndrome coronavirus. *The Journal of Biological Chemistry, 295*, 4773–4779. https://doi.org/10.1074/jbc.AC120.013056

Grein, J., Ohmagari, N., Shin, D., Diaz, G., Asperges, E., Castagna, A., et al. (2020). Compassionate use of remdesivir for patients with severe Covid-19. *The New England Journal of Medicine, 382*, 2327–2336. https://doi.org/10.1056/NEJMoa2007016 [e-pub ahead of print].

Job, P. (1928). Formation and stability of inorganic complexes in solution. *Annales de Chimie, 10*, 113–203.

Kondo, S., Ohtaki, A., Tonozuka, T., Sakano, Y., & Kamitori, S. (2001). Studies on the hydrolyzing mechanism for cyclodextrins of thermoactinomyces vulgaris R-47 α-Amylase 2 (TVAII). X-ray structure of the mutant E354A complexed with β-cyclodextrin, and kinetic analyses on cyclodextrins. *Journal of Biochemistry, 129*, 423–428. https://doi.org/10.1093/oxfordjournals.jbchem.a002873

Larson, N., (2019) Compositions comprising an RNA polymerase inhibitor and cyclodextrin for treating viral infections. US Patent US 2019/0083525, March 21, 2019.

Loftsson, T., & Brewster, M. E. (2010). Pharmaceutical applications of cyclodextrins: Basic science and product development. *The Journal of Pharmacy and Pharmacology, 62*(11). https://doi.org/10.1111/j.2042-7158.2010.01030.x

Neuhaus, D., & Williamson, M. P. (2000). *The nuclear overhauser effect in structural and conformational analysis* (2nd ed.). Wiley-VCH.

Okimoto, K., Rajewski, R. A., Uekama, K., Jona, J. A., & Stella, V. J. (1996). The interaction of charged and uncharged drugs with neutral (HP-beta-CD) and anionically charged (SBE7-beta-CD) beta-cyclodextrins. *Pharmaceutical Research, 13*(2), 256–264. https://doi.org/10.1023/a:1016047215907

Siegel, D., Hui, H. C., Doerffler, E., Clarke, O. M., Chun, K., Zhang, L., et al. (2017). Discovery and synthesis of a phosphoramidate prodrug of a Pyrrolo [2,1-f][triazin-4-amino] adenine C-Nucleoside (GS-5734) for the treatment of Ebola and emerging viruses. *Journal of Medicinal Chemistry, 60*, 1648–1661. https://doi.org/10.1021/acs.jmedchem.6b01594

Stella, V. J., & Rajewski, R. A. (2020). Sulfobutylether-β-cyclodextrin. *International Journal of Pharmaceutics, 583*, Article 119396. https://doi.org/10.1016/j.ijpharm.2020.119396

Szente, L., & Szejtli, J. (1999). Highly soluble cyclodextrin derivatives: Chemistry, properties, and trends in development. *Advanced Drug Delivery Reviews, 36*(1), 17–28. https://doi.org/10.1016/S0169-409X(98) 00092-1

Trott, O., & Olson, A. J. (2010). AutoDock Vina: Improving the speed and accuracy of docking with a new scoring function, efficient optimization, and multithreading. *Journal of Computational Chemistry, 31*, 455–461. https://doi.org/10.1002/jcc.21334

Vass, P., Démuth, B., Farkas, A., Hirsch, E., Szabó, E., Nagy, B., et al. (2019). Continuous alternative to freeze drying: Manufacturing of cyclodextrin-based reconstitution powder from aqueous solution using scaled-up electrospinning. *Journal of Controlled Release : Official Journal of the Controlled Release Society, 288*, 120–127. https://doi.org/10.1016/j.jconrel.2019.02.019, 28 March 2019.

Wang, Y., Zhang, D., Du, G., Du, R., Zhao, J., Jin, Y., et al. (2020). Remdesivir in adults with severe COVID-19: A randomised, double- blind, placebo-controlled, multicentre trial. *Lancet, 395*, 1569–1578. https://doi.org/10.1016/S0140-6736 (20) 31022-31029